Data repository

Supplementary information on the West African margin

Interpreted seismic cross-sections of the north Angolan to south Gabon west African passive margins[1-3], including the one of Figure 1 in the paper (bottom panel), that indicate similarity of structural and sedimentary features along strike on a 1000 km scale.

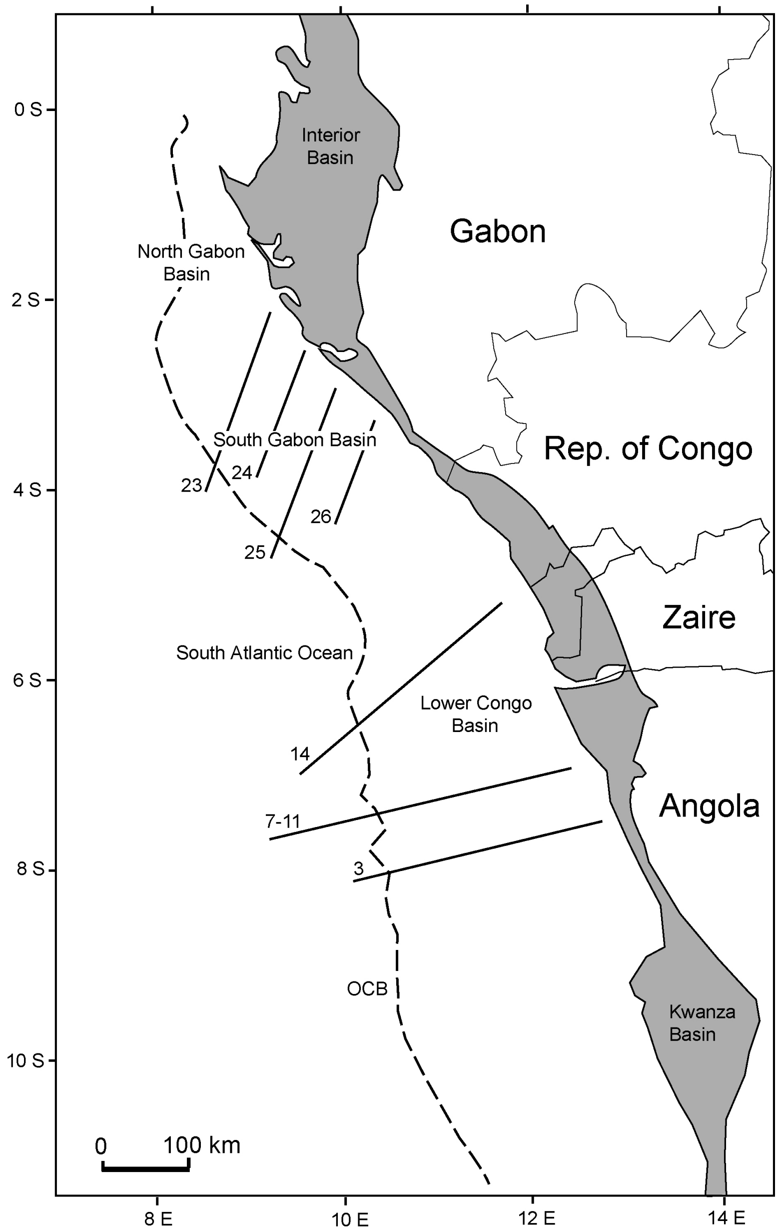

Figure DR1. Map of West African north Angolan to south Gabon margins with locations of seismic cross-sections shown in Figure DR2.

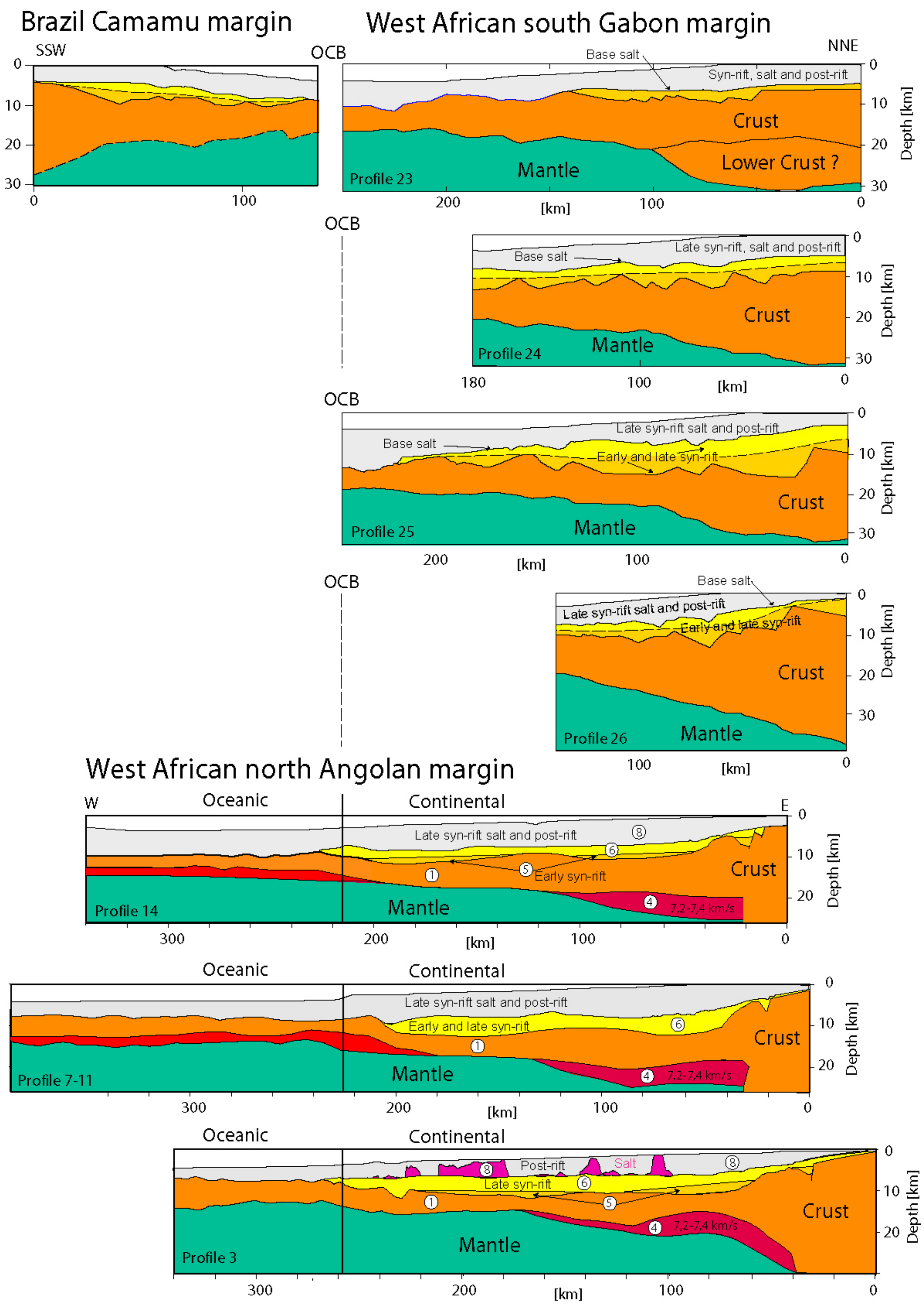

Figure DR2. Crustal cross sections from the West African north Angolan to south Gabon margins (modified after[1-3]). The crustal cross sections show wide, strongly thinned basement, thin early syn-rift deposits, thicker undeformed late syn-rift deposits, post-rift, and in the Angola sections an intermediate velocity body of unknown origin at the base of the crust. South Gabon[3] and Camamu[2] sections have been depth converted from original TWTT sections. The boundary between early and late syn-rift in these sections is not well imaged and approximately given by dashed line.

Supplementary Information on Predictions from Kinematic Extension Models

1 D prediction for the syn- and post-subsidence of sedimentary basins of the Uniform and the Depth-Dependent Extension models are given in Figure DR3.

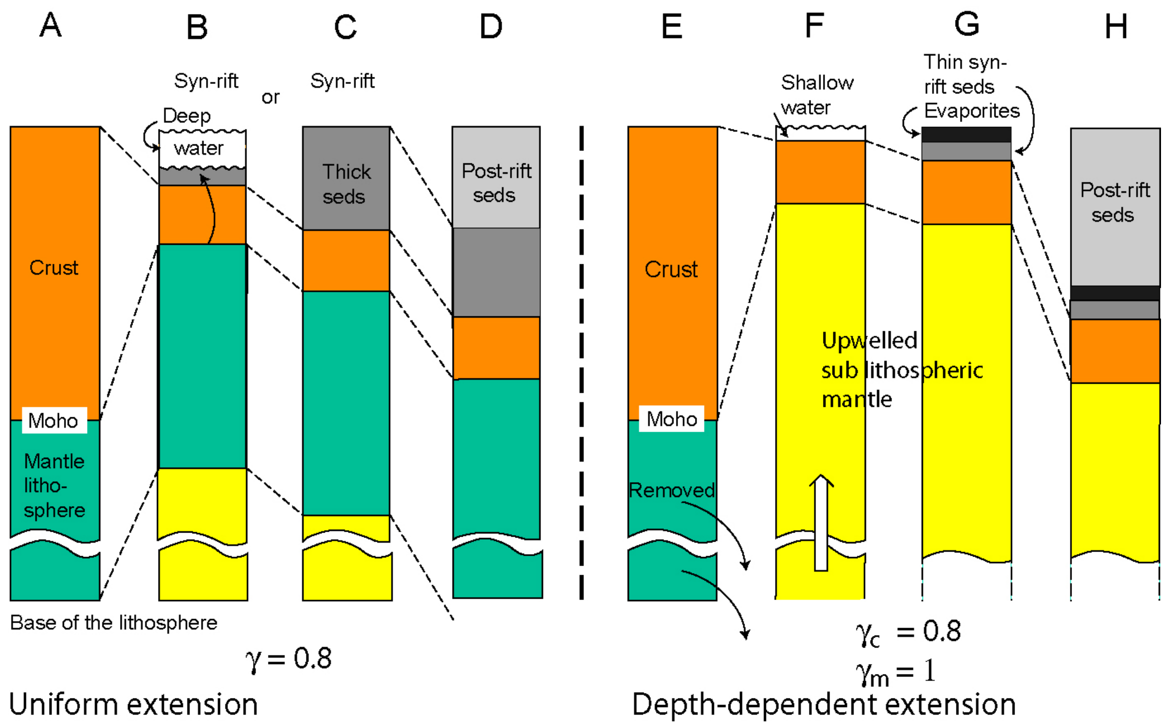

Figure DR3. 1D Predictions of evolution of Uniform (A-D) and Depth-Dependent Extension models (E-H). A) For uniform extension, large lithospheric stretching (attenuation) leading to thin crust results in either, B) thin deep-water syn-rift sediments, or C) thick sedimentary section if the upper part is required to be shallow water deposits, predictions not consistent with observations from our type example (Fig. 1) and described in text. The observed relatively thin syn-rift sediments capped by shallow water deposits are more compatible with E) depth-dependent lithospheric extension, which predicts less syn-rift subsidence F) and thinner deposits G) if the mantle lithosphere (±lower crust) is thinned disproportionately more relative to the upper/mid crust during rifting. Crust and mantle attenuation factors defined by $\gamma_c(x) = 1 - 1/\delta(x)$ and $\gamma_m(x) = 1 - 1/\beta(x)$, where $\delta(x)$ and $\beta(x)$ are the crustal and mantle lithosphere thinning factors, $h_{0c}/h_c(x)$ and, $h_{0m}/h_m(x)$.

Supplementary Information on Numerical Modelling Approach

We use an Arbitrary Lagrangian-Eulerian (ALE) finite element method for the solution of thermo-mechanically coupled, plane-strain, incompressible viscous-plastic creeping flows [4-6] to investigate extension of a layered lithosphere with frictional-plastic and thermally activated power-law viscous rheologies (Figure DR4).

When the state of stress is below the frictional-plastic yield the flow is viscous and is specified by temperature-dependent non-linear power law rheologies based on laboratory measurements on 'wet' quartzite [7] and 'wet' and 'dry' olivine [8]. The effective viscosity, η, in the power-law model is of the general form:

$$\eta = A^{-1/n} (\dot{I}_2^{\prime})^{(1-n)/2n} \exp\left[\frac{Q+Vp}{nRT}\right] \qquad (1)$$

where $\dot{I}_2^{\prime}$ is the second invariant of the deviatoric strain rate tensor ($\tfrac{1}{2}\dot{\varepsilon}_{ij}^{\prime}\dot{\varepsilon}_{ij}^{\prime}$), n is the power law exponent, A is the scaling factor, Q is the activation energy, V is the activation volume, which makes the viscosity dependent on pressure, p, T is the absolute temperature, and R is the universal gas constant. A (converted from the laboratory strain geometry to the tensor invariant form), n, Q and V are derived from the laboratory experiments and the parameter values are listed in Table DR1. Note setting $V = 0$ for the quartzite flow law does not lead to significant errors because the pressure in the crust is low.

The reference parameter values for wet quartz, listed in Table DR1, lead to a weak viscous lower crust. Very weak crust in Models 1 and 2 is achieved by decreasing $\eta_{wet\ quartz}$ by a scale factor of 10. This viscosity scaling represents a simple technique that creates very weak viscous lower crust without recourse to additional flow laws, each with its own uncertainties. The scaling can be interpreted as a measure of the uncertainty in the flow properties of rocks where flow is dominated by quartz or to be the consequence of strain softening during deformation. Sensitivity to mantle lithosphere strength is examined by using either a nominal dry or wet power law olivine viscous flow law.

The frictional-plastic deformation is modelled with a pressure-dependent Drucker-Prager yield criterion which is equivalent to the Coulomb yield criterion for incompressible deformation in plane-strain. Yielding occurs when:

$$\sigma_y = (J_2^{/})^{1/2} = C\cos\phi_{eff} + p\ Sin\,\phi_{eff} \tag{2}$$

where $J_2^{/} = \frac{1}{2}\sigma_{ij}^{/}\sigma_{ij}^{/}$ is the second invariant of the deviatoric stress, C is the cohesion, and ϕ_{eff} is the effective internal angle of friction. With appropriate choices of C and ϕ_{eff} this yield criterion can approximate frictional sliding in rocks and the effect of pore-fluid pressures. Plastic flow is incompressible. Strain softening is introduced by a linear decrease of $\phi_{eff}(\varepsilon)$ from 15º-2º (Figure DR4c and Table DR1). Note that $\phi_{eff}(\varepsilon)$ ~ 15º corresponds to the effective ϕ when the pore fluid pressure is approximately hydrostatic.

In addition to solving the equilibrium equations for viscous plastic flows in two dimensions, we also solve for the thermal evolution of the model. The mechanical and thermal systems are coupled through the temperature dependence of viscosity and density and are solved sequentially during each model time step. The initial temperature field is laterally uniform, and increases with depth from the surface, T_0 = 0 ^oC, to base of crust, T_m = 550 ^oC, following a stable geotherm for uniform crustal heat production, A_R = 0.9 $\mu W/m^3$ and a basal heat flux, q_m = 19.5 mW/m^2. Geothermal gradients, 8.6 $^oC/km$, and 0.5 $^oC/km$ (adiabatic) are uniform in the mantle lithosphere and sub-lithospheric mantle. Thermal boundary conditions are specified basal temperature, 1567 ^oC, and insulated lateral boundaries. Thermal diffusivity, $\kappa = k/\rho c_p = 10^{-6}\ m^2/s$. Densities of crust and mantle at 0 ^oC are, respectively, $\rho_{0c} = \rho_c(T_0)$ = 2800 kg/m^3 and $\rho_{0m} = \rho_m(T_0)$ = 3300 kg/m^3, and depend on temperature with a volume coefficient of thermal expansion $\alpha_T = 3.1 \times 10^{-5}\ /^oC$, $\rho(T) = \rho_0\ [1 - \alpha_T\ (T-T_0)]$.

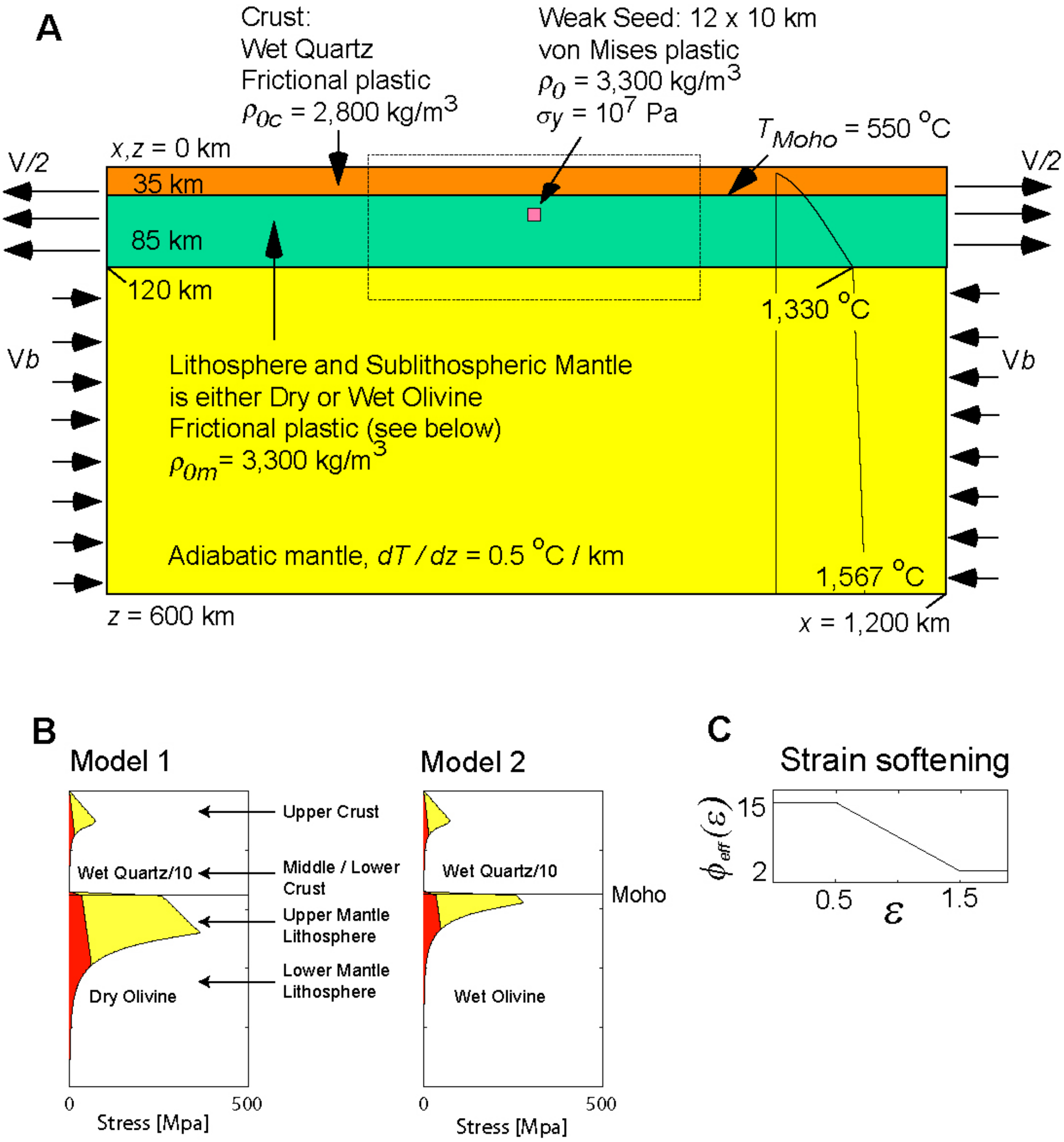

Figure DR4. Numerical model design. A) Initial crust and mantle lithosphere layer thicknesses are respectively 35 km and 85 km. Total extension velocity V = *1.0 cm/yr*. Materials deform viscously except when the material is at plastic yield. **B)** Rheological stratification for Models 1 and 2 for a nominal strain rate of 10^{-15} s^{-1}. **C)** Strain softening of frictional-plastic rheology occurs as a parametric function of total strain. Initial and strain softened friction angle, $\phi_{eff}, 15^{\circ} \rightarrow 2^{\circ}$.

Supplementary numerical models of lithosphere extension

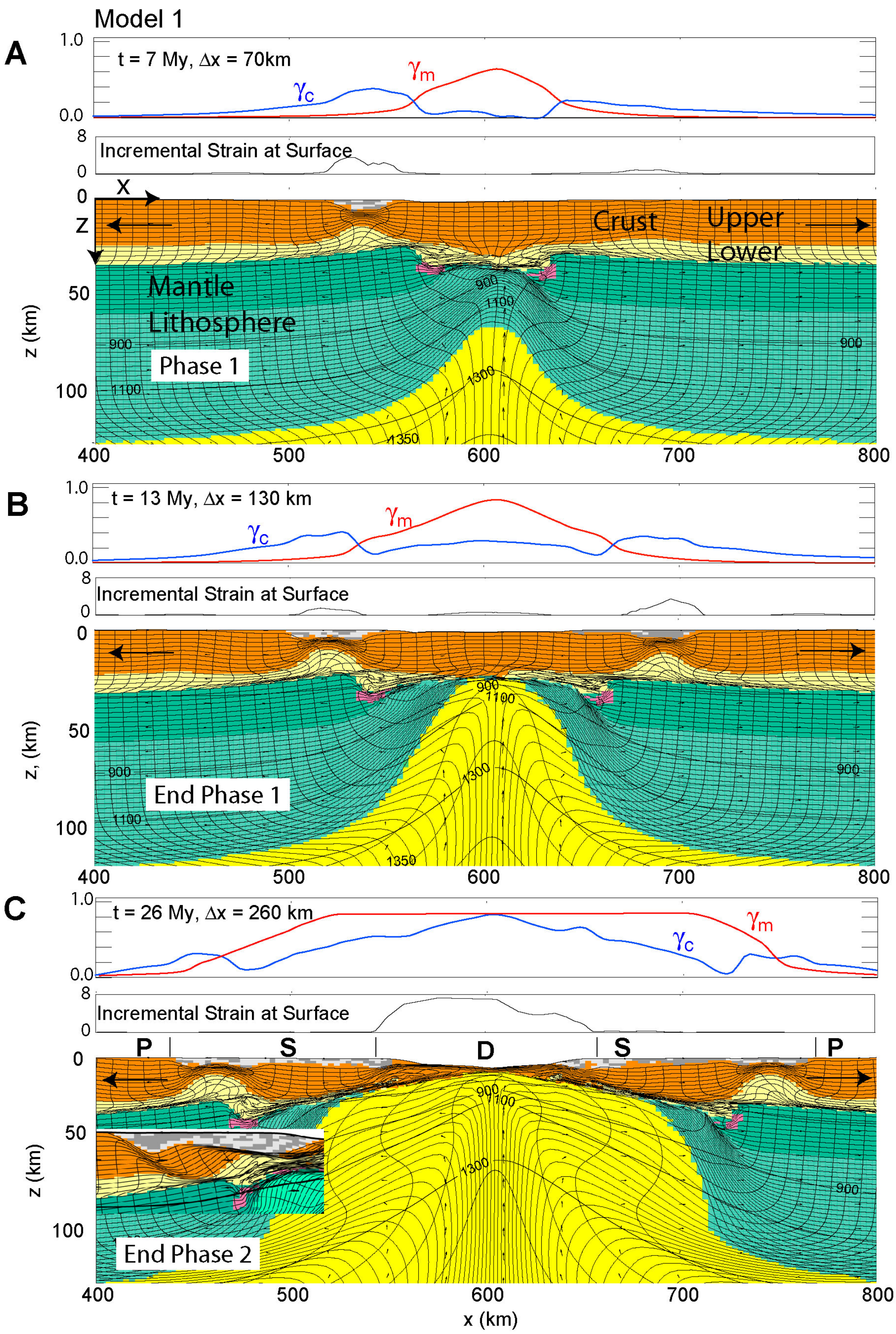

Figure DR5. Model 1. High resolution version of Figure 2. A, B, Phase 1, wide crustal rifting and narrow mantle lithosphere necking. **C**, Phase 2 crustal extension focussed in the distal margin, and progradation of sediments over non-deforming proximal parts of the rift zone. Panels show deformed Lagrangian mesh, velocity vectors, isotherms.

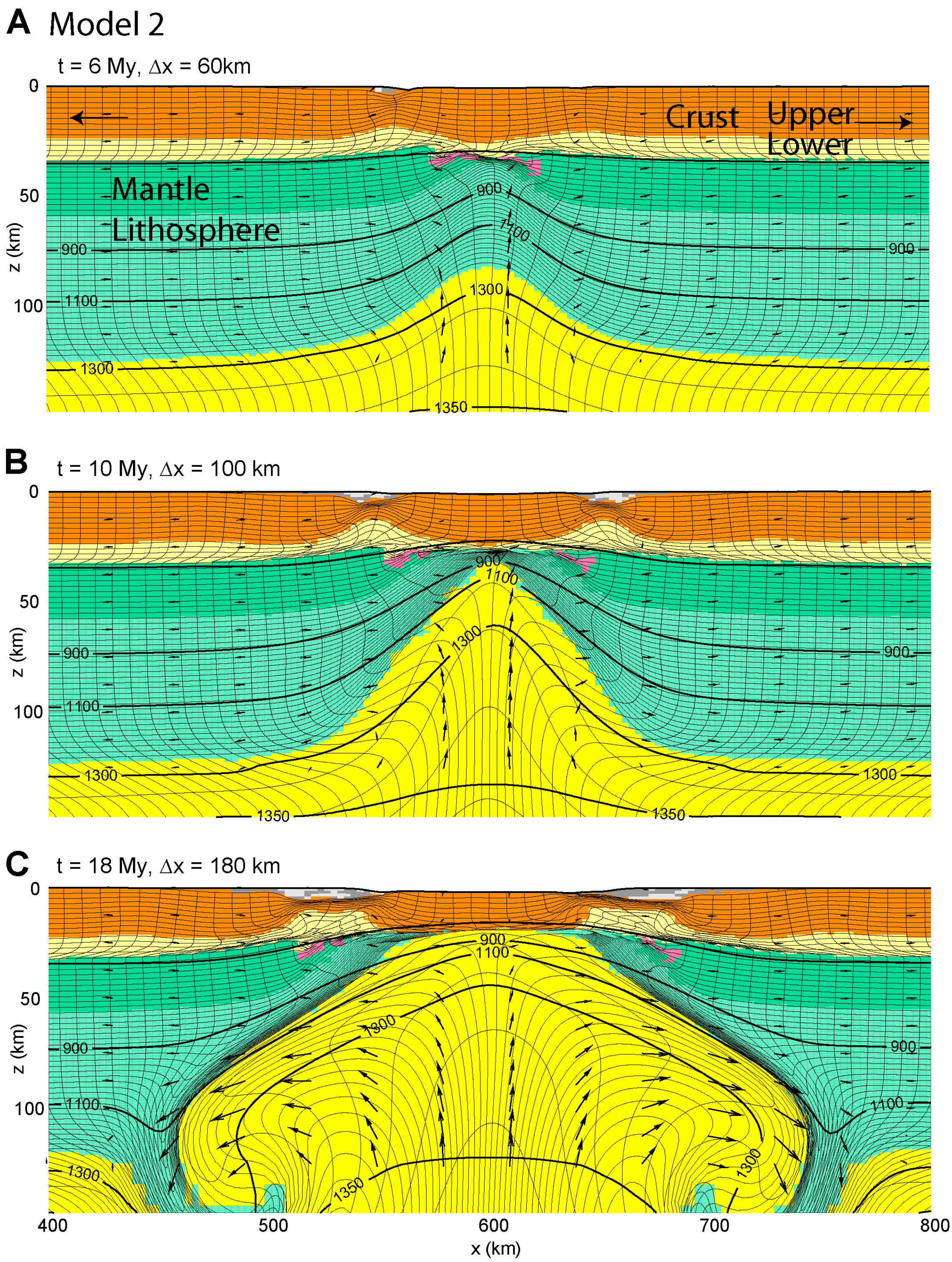

Figure DR6. Model 2 Weak Mantle Lithosphere. A, B, Phase 1, wide crustal rifting and narrow mantle lithosphere necking. **C**, Phase 2 crustal extension focussed in the distal margin, convective removal of mantle lithosphere, and progradation of sediments over non-deforming proximal parts of the rift zone. Panels show deformed Lagrangian mesh, velocity vectors, isotherms.

A full page version of Model 1 is included here (Figure DR5) so that details on model passive margin evolution can be better observed. Model 1 has a very weak crust and the crust is almost totally decoupled, $\eta = \eta_{wet\ quartz} / 10$. Details of the model evolution are described in the main text.

Model 2 has a very weak crust and the crust is almost totally decoupled as in Model 1, $\eta = \eta_{wet\ quartz} / 10$ and only differs from it in regard to its reduced mantle lithosphere viscosity ($\eta = \eta_{wet\ olivine}$). The results (Figure DR6) are similar to those for Model 1 (Figure DR5) except that the enhanced mantle necking instability and the small scale convection lead to both more rapid removal of the mantle lithosphere and its removal over a somewhat wider region. Convective removal also means that crust and mantle lithosphere extension no longer balance. These particular models are nearly symmetric, but sensitivity tests show that lithospheric heterogeneities and/or strain softening will likely offset the breakup position from the rift centre. Models 1 and 2 are purposely simple and have a single compositional layer crust A strong lower crust, for example between 35 and 40 km deep (Figure DR4) will deform in almost the same way as the upper mantle lithosphere in Models 1 and 2.

Table DR1. Parameters Lithosphere Scale Thermo-Mechanical Models.

Parameter	Symbol	Value
Rheological Parameters		
Angle of internal friction	*$\phi_{eff}(\varepsilon)$ and strain range of softening,* $(\varepsilon = \sqrt{I_2'})$	15° - 2°, 0.5-1.5
Cohesion	C	0 Pa
Wet Quartz [7]		
Power law exponent	n	4.0
Activation Energy	Q	223 x 10^3 J/mol
Initial Constant*	A	1.10 x 10^{-28} Pa^{-n}/s
Activation Volume	V	0 m^3/mol
Dry Olivine [8]		
Power law exponent	n	3.5
Activation Energy	Q	540 x 10^3 J/mol
Initial Constant*	A	2.4168 x 10^{-15} Pa^{-n}/s
Activation Volume	V	25 x 10^{-6} m^3/mol
Wet Olivine [8]		
Power law exponent	n	3.0
Activation Energy	Q	430 x 10^3 J/mol
Initial Constant*	A	1.7578 x 10^{-14} Pa^{-n}/s
Activation Volume	V	15 x 10^{-6} m^3/mol
Universal Gas Constant	R	8.3144 J/mol /°C
Thermal Parameters		
Diffusivity	κ	1 x 10^{-6} m^2/s
Crustal radioactive heat production	A_R	0.9 x 10^{-6} W/m^3
Volume coefficient of thermal expansion	α_T	3.1 x 10^{-5} /°C
Surface Temperature	T_0	0 °C
Initial Moho Temperature	T_m	550 °C

Base Lithosphere Temperature	T_L	1330 °C
Basal Temperature	T_a	1567 °C
Densities (T_0 = 0 ºC)		
Crustal density	$\rho_c(T_0)$	2800 kg/m^3
Mantle lithosphere density	$\rho_m(T_0)$	3300 kg/m^3
Sub lithospheric mantle density	$\rho_m(T_0)$	3300 kg/m^3
Dimensions and Boundary Condition		
Base of Crust		35 km
Base Mantle Lithosphere		120 km
Base Upper Mantle		600 km
Extension velocity	V	1.0 cm/y (full rate)
Top boundary condition		Stress free surface
Side boundary conditions		Free slip, normal velocity V
Basal boundary conditions		Free slip, zero normal velocity

* Values of A have been converted from the experimental values to values appropriate for plane-strain conditions.

References:

1. Moulin, M. et al. Geological constraints on the evolution of the Angolan margin based on reflection and refraction seismic data (ZaıAngo project). Geophys. J. Int. 162, 793-810 (2005).
2. Rosendahl, B. R., Mohriak, W. U., Odegard, M. E., Turner, J. P. & Dickson, W. G. in Petroleum Systems of Divergent Margin Basins (eds. Post, P. et al.) 261-317 (25th GCSSEPM Bob F. Perkins Research Conference, Houston, 2005).
3. Meyers, J. B., Rosendahl, B. R. & Austin, J. A., Jr. Deep-penetrating MCS images of the South Gabon Basin: implications for rift tectonics and post-breakup salt remobilisation. Basin Research 8, 65-84 (1996).
4. Fullsack, P. An arbitrary Lagrangian-Eulerian formulation for creeping flows and applications in tectonic models. Geophys. J. Int. 120, 1-23 (1995).
5. Willett, S. D. Rheological dependence of extension in wedge models of convergent orogens. Tectonophysics 305, 419-435 (1999).
6. Huismans, R. S. & Beaumont, C. Asymmetric lithospheric extension: relative importance of frictional-plastic and viscous strain softening inferred from numerical experiments. J. Geophys. Res. 108, doi: 10.1029/2002JB002026 (2003).
7. Gleason, G. C. & Tullis, J. A flow law for dislocation creep of quartz aggregates determined with the molten salt cell. Tectonophysics 247, 1-23 (1995).
8. Karato, S. & Wu, P. Rheology of the upper mantle. Science 260, 771-778 (1993).